Sb2S3 as a low-loss phase-change material for mid-IR photonics

Adam Biegański, Marko Perestjuk, Rémi Armand, Alberto Della Torre, Capucine Laprais, Guillaume Saint-Girons, Vincent Reboud, Jean-Michel Hartmann, Jean-Hervé Tortai, Antonin Moreau, et al.

Research Article | Vol. 14, No. 4 / 1 Apr 2024 / Optical Materials Express 862

Optical Materials EXPRESS

Sb_2S_3 as a low-loss phase-change material for mid-IR photonics

Adam Biegański,[1,2] Marko Perestjuk,[1,2] Rémi Armand,[1] Alberto Della Torre,[1] Capucine Laprais,[1] Guillaume Saint-Girons,[1] Vincent Reboud,[3] Jean-Michel Hartmann,[3] Jean-Hervé Tortai,[4] Antonin Moreau,[5] Julien Lumeau,[5] Thach Nguyen,[2] Arnan Mitchell,[2] Christelle Monat,[1] Sébastien Cueff,[1] and Christian Grillet[1,*]

[1]*CNRS, ECL, INSA Lyon, UCBL, CPE, INL UMR5270, 69134 Ecully, France*
[2]*Integrated Photonics and Application Centre (InPAC), School of Engineering, RMIT University, Melbourne, VIC 3001, Australia*
[3]*Université Grenoble Alpes, CEA-Leti, 38054 Grenoble, France*
[4]*Univ. Grenoble Alpes, CNRS, CEA/LETI-Minatec, Grenoble INP, Institute of Engineering and Management University Grenoble Alpes, LTM, Grenoble F-38054, France*
[5]*Aix Marseille Univ, CNRS, Centrale Marseille, Institut Fresnel, UMR 7249, 13013 Marseille, France*
[*]*christian.grillet@ec-lyon.fr*

Abstract: We study the mid-IR optical properties of Sb_2S_3 – a phase-change material (PCM) with high potential for mid-IR integrated photonics. We show that Sb_2S_3 exhibits a high refractive index contrast $\Delta n \approx 1$ between its two phases and an extinction coefficient k below 10^{-2} at mid-IR wavelengths (up to ~10 μm). We study the impact of 100 nm Sb_2S_3 cladding on SiGe-on-Si waveguides and experimentally show that it brings additional propagation loss below 1 dB/cm in the 3.3–3.9 μm wavelength range in both phases. These findings pave the way for new uses of Sb_2S_3 in mid-IR integrated photonics.

1. Introduction

Mid-IR wavelength range (commonly defined as spanning from 3 to 13 μm) covers the molecular absorption region of various atmospheric gases. Consequently, mid-IR integrated photonics, i.e. the integration of complex and advanced optical functionalities onto a chip, represents a promising avenue for the development of compact, cost-effective instruments for spectroscopy-based gas detection [1–6]. These structures are commonly fabricated with lithographic techniques which limit the reconfigurability and tunability of the resulting devices. Some trimming post-process capabilities were demonstrated by coating an additional layer on top of dielectric waveguides [7]. To go even further and enable a genuine post-fabrication tuning mechanism for these structures, one attractive approach is to integrate them in a hybrid manner with phase-change materials (PCMs). These materials can be reversibly switched between amorphous and crystalline phases exhibiting distinct optical properties.

Well-known examples of conventional PCMs are $Ge_2Sb_2Te_5$ (GST) [8,9] and VO_2 [10–14]. GST has been attracting intense attention due to its exceptional features, including a high refractive index contrast in the near-IR range between its two phases ($\Delta n > 2.5$), low switching temperature (~180°C) and its ability to maintain its state without any power supply. Numerous integrated devices operating around the telecom C-band such as optical memories [15], mode converters [16], reflection modulators [17], ring resonators [18], narrow-band filters [19] or phase shifters [20] based on GST were demonstrated. However, despite continuous studies and efforts to enhance its potential, its usability is still limited mostly to applications demanding light

#511923 https://doi.org/10.1364/OME.511923
Journal © 2024 Received 10 Nov 2023; revised 2 Feb 2024; accepted 2 Feb 2024; published 4 Mar 2024

Optical Materials EXPRESS

amplitude modulation [21,22]. GST in crystalline phase shows sizeable extinction coefficient throughout the mid-IR range, resulting in substantial material absorption [19]. It is therefore not suitable for low loss applications. A successful integration of PCMs with low-loss mid-IR photonics could open the door to a new realm of applications and possibilities but until now has not been demonstrated.

Recently, new attractive PCMs emerged such as $Ge_2Sb_2Se_4Te$ (GSST) [23–25], $Ge_2Sb_2Te_3S_2$ (GSTS) [26], Sb_2S_3 or Sb_2Se_3 [27–29] with the potential to be employed in low-loss devices. Particular interest was dedicated to Sb_2S_3 as it manifests significantly higher figure of merit (defined as $\Delta n/k_c$ where k_c stands for the extinction coefficient in the crystalline state) than GST while keeping similar phase switching time in the order of nanoseconds. Its potential was illustrated in image displays [30,31] and various integrated tunable devices [32–34]. Nonetheless, all demonstrations so far are limited to devices operating in the visible or near-IR wavelength range (i.e. below 2 µm). Until now, optical properties of Sb_2S_3 in terms of refractive index contrast and propagation loss in the mid-IR have not been studied. Furthermore, the thickness of the Sb_2S_3 layer in low-loss devices typically does not exceed a few tens of nanometers, thereby severely constraining the range of tunability. Optical properties of Sb_2S_3 layers of different thickness were studied up to 2.5 µm in Ref. [35] but no device operating with Sb_2S_3 claddings thicker than 100 nm was demonstrated.

In this paper, we present the first studies of Sb_2S_3 optical properties in the mid-IR range and examine its suitability for low-loss integrated tunable photonic devices. We perform spectroscopic ellipsometry measurements in both amorphous and crystalline phases for a broad wavelength range, between 560 nm and 10 µm, i.e. deep into the mid-IR band. Next, we integrate this PCM onto mid-IR waveguides, by depositing a 100 nm thick Sb_2S_3 cladding on top of SiGe-on-Si waveguides. By measuring their optical transmission in the mid-IR (3.3 to 3.9 µm) before and after crystallizing the Sb_2S_3 material, we demonstrate that a PCM cladding in both phases introduces relatively low additional loss. This shows that Sb_2S_3 is a highly promising PCM for tunable mid-IR photonic applications.

2. Ellipsometry measurements on a Sb_2S_3/Si wafer

First, we study the properties of Sb_2S_3 onto bare Si wafers. An amorphous Sb_2S_3 layer was deposited using electron-beam physical vapor deposition (EBPVD) at room temperature with a deposition rate ~0.5 Å/s, an initial pressure of 1.5×10^{-6} mbar and an emission current of 5 mA. To facilitate the ellipsometry results analysis, the structure was not capped. Thicknesses of the PCM layer before and after crystallisation were first examined by X-ray reflectometry (XRR) and found to be 101.4 nm and 90.6 nm respectively. Mid-IR optical properties were studied using the IMPACT OPTICS Ellipsometry module. For the purpose of avoiding surface oxidization, sample's crystallization was performed under vacuum, with a partial pressure of N_2 (1 mbar), in-situ in the ellipsometer chamber by heating up to the temperature of 270°C with a ramp rate of 10°C/min. Ellipsometry response of the sample at an incident angle of 70° was measured in the 350 nm−2 µm range with an Uvisel2TM and in the 2 µm−10 µm range with a MIR polarimeter. Refractive index change in amorphous and crystalline Sb_2S_3, as extracted from the fits, is shown in Fig. 1. Details of the XRR and ellipsometry measurements can be found in the Supplement 1.

Numerical values for different wavelengths are presented in Table 1. The refractive index is always higher in the crystalline phase. The refractive index contrast Δn between crystalline and amorphous Sb_2S_3 varies between 0.80 (λ=2.0 µm) and 1.00 (λ=10 µm). The extinction coefficient is found to vanish below the detection threshold ($k < 10^{-2}$) of the ellipsometer for wavelengths beyond 815 nm for both phases.

Optical Materials EXPRESS

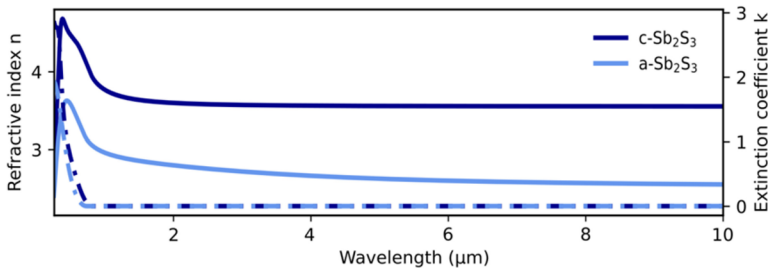

Fig. 1. Sb_2S_3 on Si wafer refractive index n (solid lines) and extinction coefficient k (dashed lines) ellipsometry measurements results in both phases from 260 nm to 10 μm.

Table 1. Sb_2S_3 refractive index *n* in amorphous and crystalline phases for selected wavelengths.

Wavelength	2 μm	4 μm	6 μm	8 μm	10 μm
n (amorphous)	2.80	2.66	2.60	2.57	2.55
n (crystalline)	3.60	3.56	3.56	3.56	3.55
Δn	0.80	0.90	0.94	0.99	1.00

3. Optical characterisation of Sb_2S_3/SiGe/Si waveguides

In the next part, we integrated a Sb_2S_3 cladding layer onto a photonic chip containing SiGe-on-Si waveguides. By performing cut-back measurement, we studied the influence of PCM layer in both phases on waveguides propagation loss.

3.1. Photonic chip description and fabrication

Photonic chip was manufactured on a 200 mm CMOS pilot line in CEA-LETI Grenoble. In the fabrication process, a 3.3 μm thick $Si_{0.6}Ge_{0.4}$ layer was grown on top of a Si substrate by Chemical Vapour Deposition (CVD) and encapsulated by a 550 nm thick Si layer. The surface roughness was removed by chemical mechanical polishing, resulting in a 50 nm thick Si encapsulation layer. Waveguides were then patterned by deep UV photolithography (DUV) followed by reactive ion etching (RIE). A Ge concentration of 40% was chosen for optimal trade-off between high nonlinear properties, transparency window and low propagation loss. Detailed fabrication procedures for the photonic chip can be found in the supplementary information of Ref. [36]. A 100 nm thick Sb_2S_3 layer was deposited following the same procedure as described in Section 2. To avoid Sb_2S_3 surface oxidization that would result in material's properties degradation, the sample was covered by EBPVD with a 9 nm thick SiO_2 capping layer. A schematic of the waveguide cross section and a scanning electron microscope (SEM) picture after the crystallization are presented in Fig. 2. As is evident on the SEM image, the deposition of the Sb_2S_3 layer exclusively occurs atop the waveguides, leaving sidewalls uncovered.

Based on the refractive index wavelength dependence presented in Section 2, we simulated the impact of a 100 nm Sb_2S_3 cladding on the waveguide properties in the mid-IR range. Figures 3(a) and 3(b) show the simulated waveguide mode effective refractive index and dispersion as a function of wavelength respectively. Figure 3 results reveal that Sb_2S_3 phase transition induces an effective refractive index and dispersion change of the order of 0.001 and 1 ps/nm/km, respectively. The limited effect can be attributed to the small confinement factor (defined in the Supplement 1) in the PCM, which does not exceed 0.14% as indicated in the intensity profile simulations presented in Fig. 4. For comparison, the overlap with the SiO_2 capping is ten times less (0.012%). We highlight that this is not an intrinsic limitation, and this could be further

Optical Materials EXPRESS

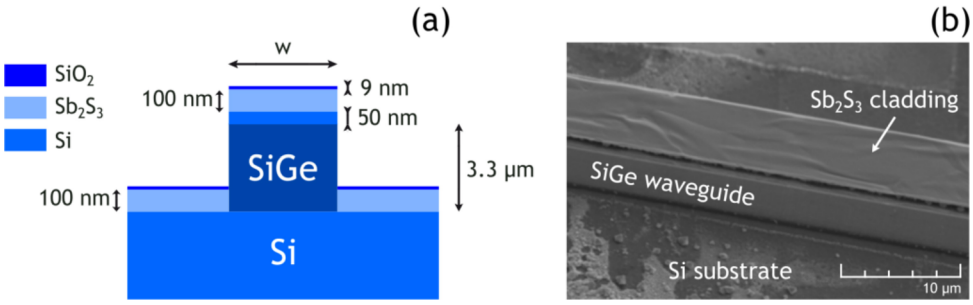

Fig. 2. **(a)** Cross section schematic and **(b)** tilted SEM picture with a 5 kV accelerating voltage of a $Si_{0.6}Ge_{0.4}$ waveguide after crystallization.

enhanced by increasing the Sb_2S_3 thickness or changing the waveguide geometry to increase the field overlap with the PCM layer.

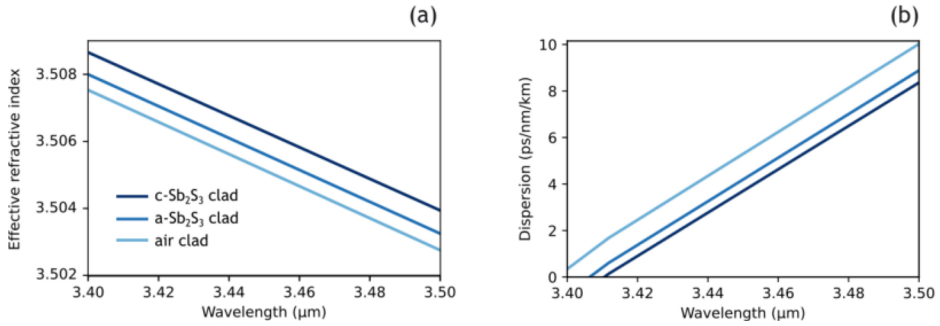

Fig. 3. Simulated **(a)** effective refractive index and **(b)** dispersion profile of the TE0 mode of the structure shown in Fig. 2(a) as a function of wavelength in the 3.40 to 3.50 μm range for air, a-Sb_2S_3 and c-Sb_2S_3 cladded $Si_{0.6}Ge_{0.4}$ waveguides. Simulations were performed with the use of Lumerical mode solver.

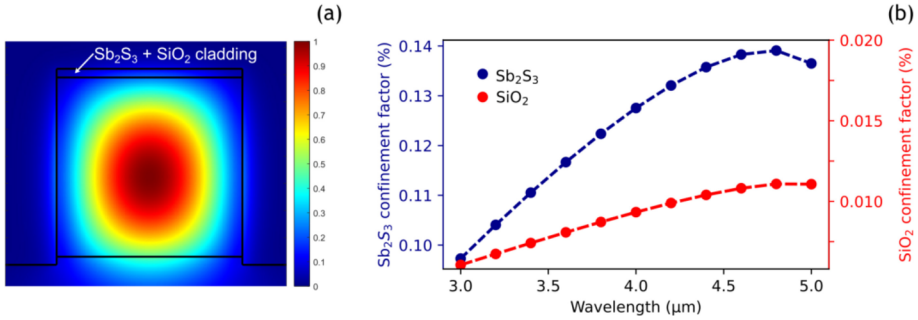

Fig. 4. Simulated **(a)** mode intensity profile (in the linear scale) of the structure for the wavelength of 3.0 μm and **(b)** calculated confined factor in the Sb_2S_3 (blue) and SiO_2 (blue) layer for the wavelength range from 3.0 to 5.0 μm.

3.2. *Propagation loss measurements*

Through numerical simulations, we find the theoretical upper limit of propagation loss in a waveguide-based geometry presented in Fig. 2(a) due to Sb_2S_3 absorption as ~2 dB/cm (associated

Optical Materials EXPRESS

with extinction coefficient k value of 10^{-2}). In order to examine the PCM cladding's influence on waveguides below the ellipsometry detection limit, we tested additional propagation loss of the PCM covered waveguides using the cut-back method on three spiral waveguides with different lengths (4.2, 6.2, and 8.2 cm, see Fig. 5). Waveguide's width and height were 3.0 µm and 3.3 µm, respectively.

Our measurement setup, shown in Fig. 6, consisted of a laser source, a half-wave plate (λ/2), two polarization controllers (PC) used for light attenuation, a chopper, two chalcogenide lenses, a PbSe photodetector and an oscilloscope. We used a tunable pulsed optical parametric amplifier (OPA, MIROPA-fs, Hotlight Systems) with a repetition rate of 63 MHz and ~200 fs pulse duration as the light source. Measurements were performed under relatively low average power (~1 mW, corresponding to the pulse peak power of 50 W) to avoid the excitation of non-linear effects and modification of the PCM properties. For wavelengths varying from 3.3 to 3.9 µm, we coupled light in the TE polarization (due to the greater sensitivity of this mode to the presence of the PCM layer) to each of the spirals and measured the output signal with a Thorlabs PDA20H-EC photodetector.

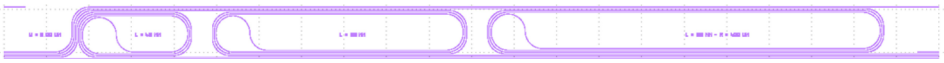

Fig. 5. Mask of spirals of different length used for propagation loss measurements.

Losses were extracted from the slope of the linear fit to the decimal logarithm of the output signal (see Fig. 7(a)). Facet and bending losses were assumed to be the same in each spiral (due to equal bending radii) so that their presence did not influence the slope. The sample's crystallization was performed by heating up to a temperature of 270°C under ambient pressure.

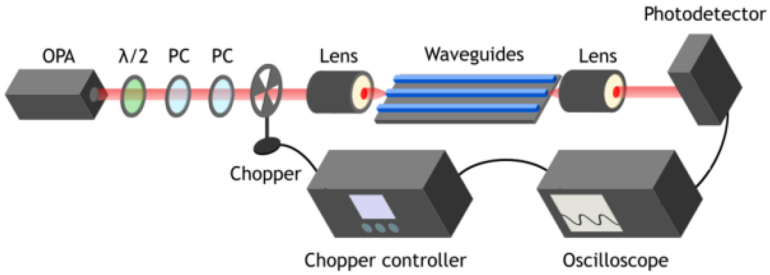

Fig. 6. Optical setup used for propagation loss measurements.

Results for air-, a-Sb_2S_3- and c-Sb_2S_3-cladded waveguides are presented in Fig. 7(b). We observe that propagation loss slightly decreases with increasing wavelengths for the three waveguide configurations, reaching around 1 dB/cm at λ = 3.9 µm. While the air- and a-Sb_2S_3-cladded waveguides yield similar loss, there is a moderate increase of propagation loss for the c-Sb_2S_3-cladded waveguide with respect to the other two.

Optical Materials EXPRESS

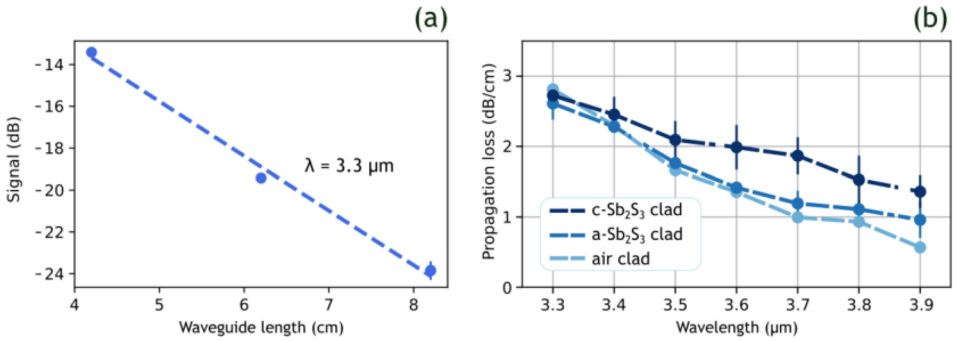

Fig. 7. **(a)** Linear fit to the output voltage signal in reference to the input signal as a function of spiral's length for 3.0×3.3 μm $Si_{0.6}Ge_{0.4}$ waveguides at a wavelength of 3.3 μm for an a-Sb_2S_3 cladding and **(b)** Propagation losses at various wavelengths for air, a-Sb_2S_3 and c-Sb_2S_3 cladded SiGe waveguides, respectively. Error bars were determined using the uncertainty associated with the least squares fit method. The dashed lines are guides for the eye.

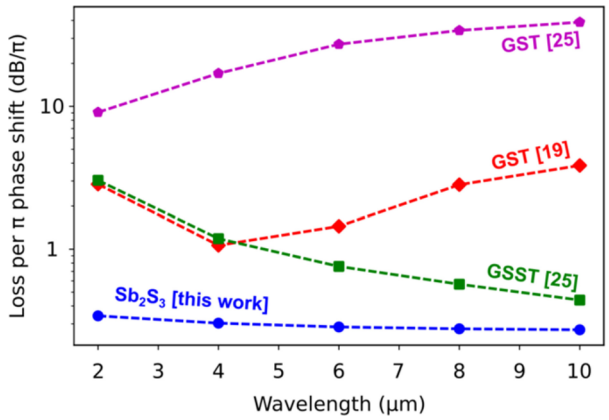

Fig. 8. Loss per π phase shift for different PCMs in the mid-IR range inferred based on ellipsometry results. Data are taken from [19] (GST red) and [25] (GSST and GST magenta). The significantly different performances of GST might stem from distinct stoichiometry or density attributed to different deposition techniques.

Optical Materials EXPRESS

4. Discussion

Propagation loss experienced by light propagating inside a PCM over a distance required to achieve a π phase shift can serve as a quantitative criterion for comparing materials in terms of their suitability for low-loss reconfigurable photonics. This can be calculated from the ellipsometry measurements of Section 2 via [20]:

$$Loss\left(\frac{dB}{\pi}\right) = \frac{20\pi}{ln10}\frac{k_c}{\Delta n} \tag{1}$$

With a refractive index contrast Δn between both phases approaching unity and an exceedingly low extinction coefficient in its crystalline phase ($k_c < 10^{-2}$), Sb_2S_3 exhibits loss per π phase shift of less than 0.3 dB beyond the wavelength of 3 μm which positions it as a leading candidate for mid-IR photonics. A comparison of loss per π phase shift for different PCMs in the mid-IR range is presented in Fig. 8.

Regarding the hybrid waveguide results, Fig. 7 measurements show that, for wavelengths between 3.3 μm and 3.9 μm, the presence of a 100 nm thick Sb_2S_3 cladding results in nearly negligible additional propagation loss in the amorphous phase, with a modest increase after crystallization. In both phases, the additional loss of the hybrid waveguide thus remains below 1 dB/cm. Considering the equally low (<0.3 dB) loss per π phase shift value, which more fairly accounts for the light interaction with the PCM, Sb_2S_3 can be deemed highly promising for a variety of low-loss devices as it represents a noteworthy combination of low propagation loss and decent tunability capability. We note that SiGe-on-Si waveguides have been shown to exhibit propagation loss as low as below 0.2 dB/cm for wavelengths beyond 3.3 μm [37]. The slightly higher absolute loss level presented in Fig. 7(b) for air-cladded waveguides may here originate from mechanical damages to the photonic chip during sample manipulation prior to the PCM deposition. It is however not an intrinsic limitation of this platform. Our results show that both contributions to loss (absorption and scattering) remain low in a c-Sb_2S_3 waveguide-based geometry, as would be used in practical device implementation. Since the extra propagation loss for the waveguide with Sb_2S_3 in the crystalline phase is lower than the theoretical upper limit predicted by simulations (2 dB/cm) considering the most pessimistic extinction coefficient of 10^{-2} (see Section 2), the current study does not allow us to identify its origin. It could stem from Sb_2S_3 residual absorption or light scattering at grain boundaries and at the Sb_2S_3/SiGe interface. A prospective avenue may involve the systematic analysis of the influence of diverse fabrication parameters such as deposition rate, capping layer thickness, crystallization temperature, pressure and so on. We next plan to test waveguides with thicker Sb_2S_3 claddings. Such configurations would be useful to increase the tunability of waveguide properties upon PCM phase changes.

These findings lead to a further extension of the operational wavelength range of tunable devices such as phase shifters or mode converters to the mid-IR. The possibility of depositing PCM claddings with thicknesses exceeding 100 nm without introducing substantial amount of additional propagation loss should lead to an enhancement of the tunability of waveguide's properties such as dispersion profile and effective refractive index, therefore significantly improving the versatility of integrated devices, including ring resonators or directional couplers. The findings can also pave the way for an entire new group of applications such as waveguide's dispersion profile modification for nonlinear light sources.

5. Conclusion

We have measured for the first time the optical properties of Sb_2S_3 thin films in the mid-IR wavelength range and demonstrated their suitability for low-loss integrated photonics in this wavelength range. Thanks to ellipsometry measurements, we showed that the refractive index contrast between a-Sb_2S_3 and c-Sb_2S_3 was high ($\Delta n \approx 1$) up to 10 μm wavelength and found

Optical Materials EXPRESS

extinction coefficients below the detection threshold ($k < 10^{-2}$) in the entire measurement range. We demonstrated that the deposition of 100 nm of Sb_2S_3 on top of SiGe-on-Si waveguides resulted in additional propagation loss below 1 dB/cm regardless of the Sb_2S_3 phase. These findings create opportunities for the use of Sb_2S_3 in reconfigurable low-loss integrated mid-IR devices.

Funding. H2020 Marie Skłodowska-Curie Actions (101034328, 801512); Agence Nationale de la Recherche (ANR-17-CE24-0028, ANR-20-CE24-0013, ANR-22-PEEL-0005).

Acknowledgments. This work benefits from a France 2030 government grant managed by the French National Research Agency (ANR-22-PEEL-0005). We acknowledge the support of the International Associated Laboratory in Photonics between France and Australia (LIA ALPhFA), the Agence Nationale de la Recherche (MIRSICOMB, ANR-17-CE24-0028; MetaOnDemand, ANR-20-CE24-0013 and MIRthFUL, ANR-21-CE24-0005), the Horizon 2020 research and innovation programme under the Marie Skłodowska-Curie Actions (MSCA) (REDI, grant agreement No 101034328 and ECLAUSion, grant agreement No 801512), the EquipEx French Government program "IMPACT" (ANR-10-EQPX-33) and the French National Nanofabrication Network Renatech.

Disclosures. The authors declare no conflicts of interest

Data availability. Data underlying the results presented in this paper are not publicly available at this time but may be obtained from the authors upon reasonable request.

Supplemental document. See Supplement 1 for supporting content.

References

1. D. Popa and F. Udrea, "Towards Integrated Mid-Infrared Gas Sensors," Sensors **19**(9), 2076 (2019).
2. T. Hu, B. Dong, X. Luo, *et al.*, "Silicon photonic platforms for mid-infrared applications [Invited]," Photonics Res. **5**(5), 417 (2017).
3. E. Tagkoudi, D. Grassani, F. Yang, *et al.*, "Parallel gas spectroscopy using mid-infrared supercontinuum from a single Si_3N_4 waveguide," Opt. Lett. **45**(8), 2195 (2020).
4. N. Nader, D. L. Maser, F. C. Cruz, *et al.*, "Versatile silicon-waveguide supercontinuum for coherent mid-infrared spectroscopy," APL Photonics **3**(3), 036102 (2018).
5. N. Nader, A. Kowligy, J. Chiles, *et al.*, "Infrared frequency comb generation and spectroscopy with suspended silicon nanophotonic waveguides," Optica **6**(10), 1269 (2019).
6. A. Della Torre, R. Armand, M. Sinobad, *et al.*, "Mid-infrared supercontinuum generation in a varying dispersion waveguide for multi-species gas spectroscopy," IEEE J. Select. Topics Quantum Electron. **1**, 1–10 (2023).
7. M. Sinobad, A. Della Torre, B. Luther-Davis, *et al.*, "Dispersion trimming for mid-infrared supercontinuum generation in a hybrid chalcogenide/silicon-germanium waveguide," J. Opt. Soc. Am. B **36**(2), A98 (2019).
8. T. Cao, R. Wang, R. E. Simpson, *et al.*, "Photonic Ge-Sb-Te phase change metamaterials and their applications," Prog. Quantum Electron. **74**, 100299 (2020).
9. M. Wuttig, H. Bhaskaran, and T. Taubner, "Phase-change materials for non-volatile photonic applications," Nat. Photonics **11**(8), 465–476 (2017).
10. S. Cueff, J. John, Z. Zhang, *et al.*, "VO_2 nanophotonics," APL Photonics **5**(11), 110901 (2020).
11. Y. Ke, S. Wang, G. Liu, *et al.*, "Vanadium dioxide: the multistimuli responsive material and its applications," Small **14**(39), 1802025 (2018).
12. K. Liu, S. Lee, S. Yang, *et al.*, "Recent progresses on physics and applications of vanadium dioxide," Mater. Today **21**(8), 875–896 (2018).
13. P. Markov, R. E. Marvel, H. J. Conley, *et al.*, "Optically monitored electrical switching in VO_2," ACS Photonics **2**(8), 1175–1182 (2015).
14. K. J. Miller, K. A. Hallman, R. F. Haglund, *et al.*, "Silicon waveguide optical switch with embedded phase change material," Opt. Express **25**(22), 26527 (2017).
15. C. Ríos, M. Stegmaier, P. Hosseini, *et al.*, "Integrated all-photonic non-volatile multi-level memory," Nat. Photonics **9**(11), 725–732 (2015).
16. C. Wu, H. Yu, S. Lee, *et al.*, "Programmable phase-change metasurfaces on waveguides for multimode photonic convolutional neural network," Nat. Commun. **12**(1), 96 (2021).
17. S. Cueff, A. Taute, A. Bourgade, *et al.*, "Reconfigurable flat optics with programmable reflection amplitude using lithography-free phase-change material ultra-thin films," Adv. Opt. Mater. **9**(2), 2001291 (2021).
18. J. Zheng, Z. Fang, C. Wu, *et al.*, "Nonvolatile electrically reconfigurable integrated photonic switch enabled by a silicon pin diode heater," Adv. Mater. **32**(31), 2001218 (2020).
19. M. N. Julian, C. Williams, S. Borg, *et al.*, "Reversible optical tuning of GeSbTe phase-change metasurface spectral filters for mid-wave infrared imaging," Optica **7**(7), 746 (2020).
20. Y. Miyatake, C. P. Ho, P. Pitchappa, *et al.*, "Non-volatile compact optical phase shifter based on $Ge_2Sb_2Te_5$ operating at 2.3 μm," Opt. Mater. Express **12**(12), 4582 (2022).
21. J. Faneca, S. Garcia-Cuevas Carrillo, E. Gemo, *et al.*, "Performance characteristics of phase-change integrated silicon nitride photonic devices in the O and C telecommunications bands," Opt. Mater. Express **10**(8), 1778 (2020).

Optical Materials EXPRESS

22. J. Parra, J. Navarro-Arenas, M. Kovylina, *et al.*, "Impact of GST thickness on GST-loaded silicon waveguides for optimal optical switching," Sci. Rep. **12**(1), 9774 (2022).
23. Y. Zhang, C. Fowler, J. Liang, *et al.*, "Electrically reconfigurable non-volatile metasurface using low-loss optical phase-change material," Nat. Nanotechnol. **16**(6), 661–666 (2021).
24. Q. Zhang, Y. Zhang, J. Li, *et al.*, "Broadband nonvolatile photonic switching based on optical phase change materials: beyond the classical figure-of-merit," Opt. Lett. **43**(1), 94 (2018).
25. Y. Zhang, J. B. Chou, J. Li, *et al.*, "Broadband transparent optical phase change materials for high-performance nonvolatile photonics," Nat. Commun. **10**(1), 4279 (2019).
26. Y. Miyatake, K. Makino, J. Tominaga, *et al.*, "Proposal of Low-Loss Non-Volatile Mid-Infrared Optical Phase Shifter Based on $Ge_2Sb_2Te_3S_2$," IEEE Trans. Electron Devices **70**(4), 2106–2112 (2023).
27. M. Delaney, I. Zeimpekis, D. Lawson, *et al.*, "A New Family of Ultralow Loss Reversible Phase-Change Materials for Photonic Integrated Circuits: Sb_2S_3 and Sb_2Se_3," Adv. Funct. Mater. **30**(36), 2002447 (2020).
28. M. Delaney, I. Zeimpekis, H. Du, *et al.*, "Nonvolatile programmable silicon photonics using an ultralow-loss Sb_2Se_3 phase change material," Sci. Adv. **7**(25), eabg3500 (2021).
29. A. Taute, S. Al-Jibouri, C. Laprais, *et al.*, "Programming multilevel crystallization states in phase-change-material thin films," Opt. Mater. Express **13**(11), 3113 (2023).
30. W. Dong, H. Liu, J. K. Behera, *et al.*, "Wide Bandgap Phase Change Material Tuned Visible Photonics," Adv. Funct. Mater. **29**(6), 1806181 (2019).
31. H. Liu, W. Dong, H. Wang, *et al.*, "Rewritable color nanoprints in antimony trisulfide films," Sci. Adv. **6**(51), eabb7171 (2020).
32. Z. Fang, J. Zheng, A. Saxena, *et al.*, "Non-Volatile Reconfigurable Integrated Photonics Enabled by Broadband Low-Loss Phase Change Material," Adv. Opt. Mater. **9**(9), 2002049 (2021).
33. P. Moitra, Y. Wang, X. Liang, *et al.*, "Programmable Wavefront Control in the Visible Spectrum Using Low-Loss Chalcogenide Phase-Change Metasurfaces," Adv. Mater. **35**(34), 2205367 (2023).
34. T. Y. Teo, M. Krbal, J. Mistrik, *et al.*, "Comparison and analysis of phase change materials-based reconfigurable silicon photonic directional couplers," Opt. Mater. Express **12**(2), 606 (2022).
35. P. Kepič, P. Liška, B. Idesová, *et al.*, "Pulsed laser deposition of Sb_2S_3 films for phase-change tunable nanophotonics," New J. Phys. **26**(1), 013005 (2024).
36. M. Sinobad, C. Monat, B. Luther-davies, *et al.*, "Mid-infrared octave spanning supercontinuum generation to 85 μm in silicon-germanium waveguides," Optica **5**(4), 360 (2018).
37. R. Armand, M. Perestjuk, A. Della Torre, *et al.*, "Mid-infrared integrated silicon–germanium ring resonator with high Q-factor," APL Photonics **8**(7), 071301 (2023).